Understanding analog quantum simulation dynamics in coupled ion-trap qubits

Yang-Le Wu[1] and S. Das Sarma[1]

[1] *Condensed Matter Theory Center and Joint Quantum Institute, Department of Physics, University of Maryland, College Park, MD 20742*

(Dated: March 1, 2016)

We study numerically a disordered transverse-field Ising Hamiltonian with long-range couplings. This model was recently investigated experimentally in a trapped-ion quantum simulator and was found to exhibit features of many-body localization at strong disorder. We use exact diagonalization to study the collective state preservation and the eigenstate entanglement structure as a function of both disorder strength and interaction range. Our numerical results, using the same system sizes as the experiment, verify the observation of many-body localization reported in the recent quantum simulation experiment, and point to directions for future experiments.

arXiv:1512.00848v2 [cond-mat.dis-nn] 29 Feb 2016

I. INTRODUCTION

Engineered systems of trapped ions allow reliable control of interaction parameters and precise measurement of local observables [1, 2]. Such analog "quantum simulators" [3] make it possible to experimentally probe the many-body dynamics of interacting quantum Hamiltonians. In a recent paper, Smith *et al.* [4] presented a quantum simulation of a one-dimensional disordered Ising model using a linear array of $N = 10$ trapped-ion qubits, and they reported the experimental observation of many-body localization (MBL) [5–10]. This disorder-induced phenomenon refers to the absence of thermalization in highly excited states of a strongly correlated, isolated quantum system, where the nonergodic time evolution fails to erase the local properties of the initial state. Due to its marked departure from the usual hypotheses of quantum statistical mechanics, the strange properties of MBL [11–16] are an intense focus of current research, as surveyed by the recent reviews [17, 18].

The study of MBL has up to now largely been driven forward by numerical calculations in finite-size systems of a few tens of spins or particles [19]. Unfortunately, they still fall short of directly addressing a fundamental issue of MBL physics, namely, whether a high-temperature thermalization-localization transition actually exists at *finite* disorder strength in an infinite system. This makes the recent experimental advances [4, 20] particularly tantalizing, as they may soon be scaled up to simulate large quantum systems well beyond the capabilities of digital simulations on classical computers.

In this paper we provide a theoretical characterization of the coupled qubit dynamics in the trapped-ion experiment [4]. Contrary to the Heisenberg model commonly studied in the MBL literature [18], the spins in the ion-trap quantum simulator are more appropriately modeled by a long-range Ising Hamiltonian [21]. This prompts us to examine the trapped-ion system carefully and verify the experimental observation with numerical calculations. Here we refrain from the attempt to tackle the (putative) localization transition in the thermodynamic limit. Instead, we focus on the qualitative differences in coherent dynamics between strong and weak disorder at small system sizes relevant to current experiments. Our work also points toward directions for future experiments with increasing system sizes.

II. DYNAMICS OF TRAPPED-ION QUBITS

We adopt from Ref. [4] the long-range effective Hamiltonian for a disordered transverse-field Ising chain of N trapped ions [21],

$$H = \sum_{i<j} J_{i,j}\sigma_i^x\sigma_j^x + \frac{1}{2}\sum_i (B + D_i)\sigma_i^z. \tag{1}$$

Here, the Ising coupling $J_{i,j} = J_{\max}/|i-j|^\alpha$ is characterized [22] by the long-range exponent α, and the disordered transverse field has site-independent mean value B and fluctuation D_i drawn independently and uniformly from $[-W, W]$. Throughout this paper, we fix $B = 4J_{\max}$ in accordance with Ref. [4], and for each system parameter we average the calculation results over 10^3 disorder realizations.

We use exact diagonalization to study the collective state dynamics and the eigenstate structure of H. We aim to probe numerically the localization transition of the trapped ions at small system sizes relevant to the trapped-ion experiment [4]. Specifically, we try to characterize the finite-size crossover through two complementary sets of localization measures, namely, the memory preservation of collective state and the structure of eigenstate entanglement.

The experiment reported in Ref. [4] tracked the time evolution of local observables of $N = 10$ trapped ions in an analog quantum simulator and studied the dependence of initial-state memory retention on disorder strength. In the following, we perform the same dynamical measurements *in silico* and try to reproduce the experimental data from numerics using the disordered Ising model in Eq. (1).

Following the experimental setup [4], we consider the Néel ordered initial state $|\psi(0)\rangle = |\uparrow\downarrow\cdots\uparrow\downarrow\rangle_z$ and study the time evolution of the collective state $|\psi(t)\rangle$. We work in the long-range interacting regime as in Ref. [4] and fix the system parameters to $\alpha = 1.13$ and $B = 4J_{\max}$

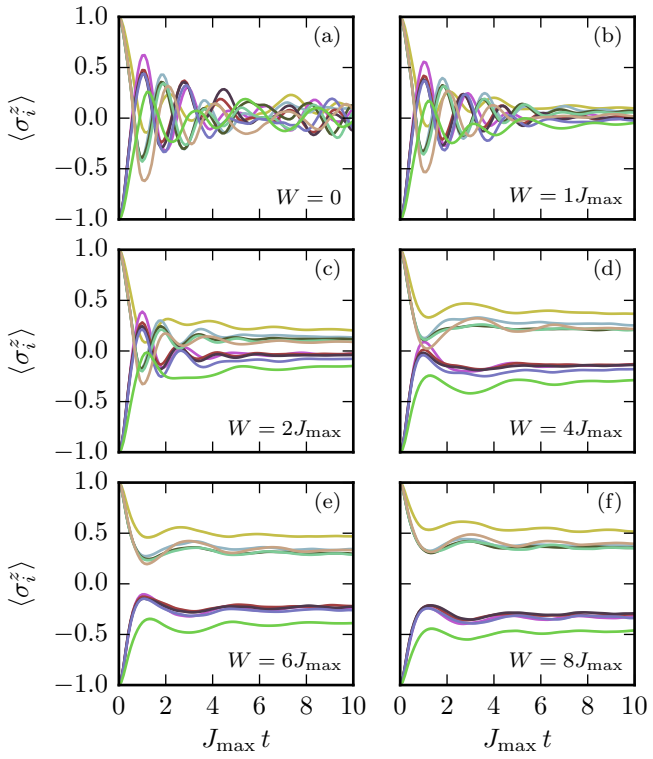

FIG. 1. Time evolution of single-site magnetization $\langle \sigma_i^z \rangle$ starting from the Néel state $|\uparrow\downarrow\uparrow\downarrow\uparrow\downarrow\uparrow\downarrow\rangle_z$ of $N = 10$ trapped ions, at $\alpha = 1.13$, $B = 4J_{\max}$, and $W \in \{0, 1, 2, 4, 6, 8\}J_{\max}$. Each curve tracks the magnetization dynamics of a single site, averaged over 10^3 disorder realizations. The standard error is smaller than the line width.

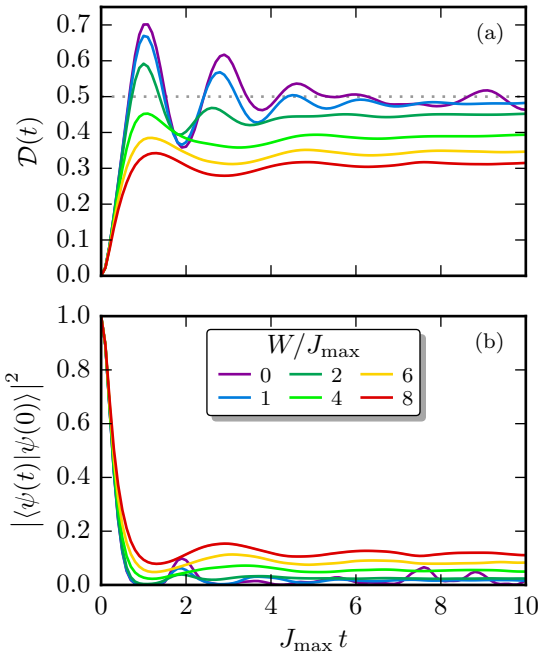

FIG. 2. Time evolution of (a) the normalized Hamming distance and (b) the return probability, starting from the Néel state $|\uparrow\downarrow\uparrow\downarrow\uparrow\downarrow\uparrow\downarrow\rangle_z$ of $N = 10$ trapped ions, at $\alpha = 1.13$, $B = 4J_{\max}$, and $W \in \{0, 1, 2, 4, 6, 8\}J_{\max}$ (color code). Each curve shows the average of 10^3 disorder realizations. The standard error is smaller than the line width.

accordingly. We tune the disorder strength W over the same set of values as in the experiment, up to $8J_{\max}$.

We quantify the collective state preservation using a combination of three different probes, namely, the single-site magnetization $\langle \sigma_i^z \rangle \equiv \langle \psi(t)|\sigma_i^z|\psi(t)\rangle$, the normalized Hamming distance $\mathcal{D}(t)$ [4, 23], and the return probability $|\langle\psi(t)|\psi(0)\rangle|^2$. The former two quantities were studied experimentally in Ref. [4]. When $|\psi(0)\rangle$ is a product state (such as the Néel state considered here), the return probability can also, in principle, be studied experimentally through a joint spin measurement.

Figure 1 shows the dynamics of single-site magnetization in the z direction at various disorder strengths W. For small W, the antiferromagnetic polarization in the initial Néel state is quickly washed away, and the system retains no long-term memory. In contrast, for $W \gtrsim 4J_{\max}$, the antiferromagnetic polarization pattern partially persists through the time evolution. Our numerical results semiquantitatively reproduce the experimentally measured magnetization curves reported in Fig. 2 of Ref. [4].

As an alternative signature of state preservation, we also examine the time evolution of the normalized Hamming distance $\mathcal{D}(t)$ from the initial state [4, 23],

$$\mathcal{D}(t) = \frac{1}{2} - \frac{1}{2N}\sum_k \langle\psi(0)|e^{iHt}\sigma_k^z e^{-iHt}\sigma_k^z|\psi(0)\rangle. \quad (2)$$

This quantity measures the deviation between the initial and the final states by counting the numbers of spin flips. For the Néel ordered initial state $|\psi(0)\rangle = |\uparrow\downarrow\cdots\uparrow\downarrow\rangle_z$, we note that the combination

$$1 - 2\mathcal{D}(t) = \frac{1}{N}\sum_k (-1)^k \langle\psi(t)|\sigma_k^z|\psi(t)\rangle \quad (3)$$

is simply the magnetization counterpart of the "atom-number imbalance" $\mathcal{I}(t)$ between even and odd sites as measured in the optical lattice MBL experiment of Ref. [20]. The Hamming distance is normalized such that for a thermalizing system with no long-term memory, $\mathcal{D}(t)$ relaxes to $1/2$ asymptotically, while for a fully localized system it stays at zero. Figure 2(a) shows that at weak disorder, $\mathcal{D}(t)$ quickly rises to $\frac{1}{2}$, indicating a total loss of memory about the initial Néel state, and as disorder increases, the asymptotic value of $\mathcal{D}(t)$ decreases steadily, signaling a gradual onset of localization. Comparing our numerical results and the experimental data in Fig. 3 of Ref. [4], we note that many features in the experimentally measured curves for $\mathcal{D}(t)$ are reproduced semi-quantitatively in our numerical results. This further

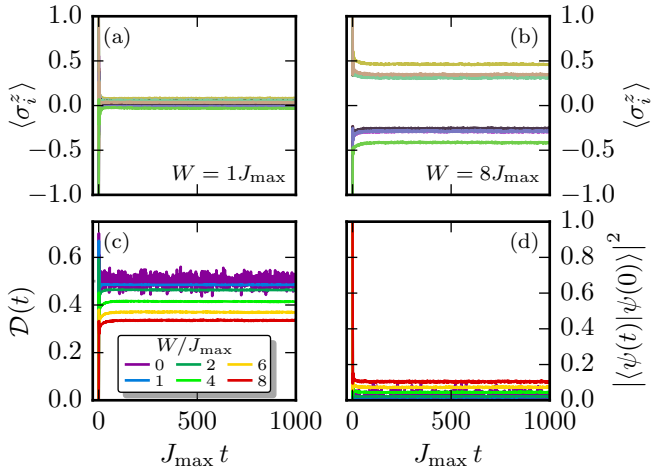

FIG. 3. Collective state preservation over an extended period of time much longer than the experimental measurement [4]. (a), (b) The dynamics of single-site magnetization, (c) the normalized Hamming distance, and (d) the return probability, using the same setup as Figs. 1 and 2.

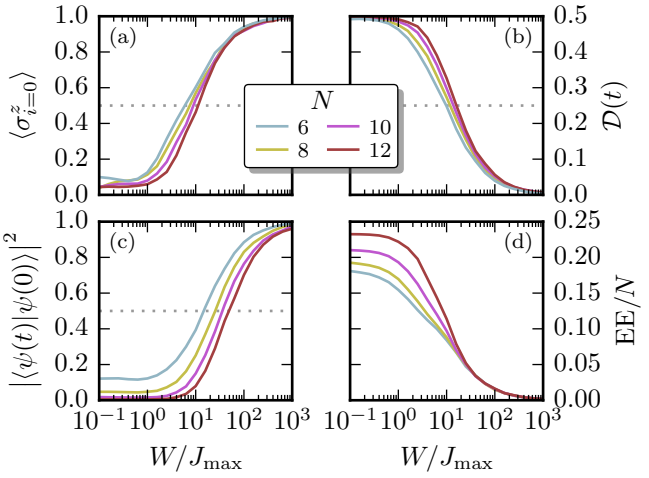

FIG. 4. Disorder dependence of localization measures, including (a) steady-state magnetization at site $i = 0$, (b) steady-state Hamming distance, (c) steady-state return probability, and (d) middle-cut entanglement entropy (EE) density, at $\alpha = 1.13$ and $B = 4J_{\max}$, averaged over 10^3 disorder realizations. For each system size N and disorder strength W, the steady-state values are obtained by averaging the time evolution over $t \in [100, 110]J_{\max}^{-1}$ starting from the Néel state $|\uparrow\downarrow\cdots\uparrow\downarrow\rangle_z$, whereas the entanglement entropy density is averaged over all eigenstates. The dotted line in panels (a)-(c) marks the halfway threshold that defines the effective critical disorder W_c at finite size.

attests to the claim of Ref. [4] that the trapped-ion quantum simulator is indeed seeing the finite-size localization crossover in the disordered Ising model.

The above two localization indicators are experimentally measurable, but, unfortunately, the memory retention of these few-body observables is not guaranteed to fully establish the preservation of the collective quantum state itself. A more stringent, albeit less experimentally accessible measure of memory retention is the return probability $|\langle\psi(t)|\psi(0)\rangle|^2$. Figure 2(b) shows the evolution of the return probability at different disorder strengths. We find that at weak disorder, the return probability quickly dies off, consistent with the thermalizing behavior of the dynamics of magnetization as well as the Hamming distance. As disorder strengthens, the asymptotic return probability increases steadily. Nevertheless, even at the strongest disorder $W = 8J_{\max}$ tested in Ref. [4], the return probability is still far from unity. This indicates that the finite-size crossover from thermal to localized phases for $N = 10$ trapped ions occurs at an even stronger disorder, as we will see later.

As a final check on the experimental results, we study the asymptotic behavior of memory retention. In the actual quantum simulator device, the chain of trapped ions is not a perfectly isolated system, and the decoherence due to the inevitable coupling to the environment limits the maximum duration of the dynamical measurement to a relatively short time period $\sim 10J_{\max}^{-1}$ [4]. In contrast, our digital simulation can be continued indefinitely, allowing us to check whether the state preservation is genuine or an artifact from limited measurement duration. As shown in Fig. 3, we find that the three different measures of memory retention all quickly approach a steady state, and their asymptotic values do not differ significantly from $t \sim 10J_{\max}^{-1}$. This shows that the memory retention observed experimentally in Ref. [4] can indeed be attributed to the collective state preservation effect of MBL.

We now expand our calculations to cover a wider range of disorder strengths and system sizes, up to $N = 12$ sites. We still consider the regime with long-range Ising coupling at $\alpha = 1.13$. Limited by the cost of numerical diagonalization, we are not able to directly probe the many-body localization phase transition, which is a sharp transition only in the thermodynamic limit $N \to \infty$. Instead, we seek to investigate the finite-size crossover between the thermal phase and the localized phase for small systems.

We quantify localization, or more precisely the lack of ergodicity, using the three measures of collective state preservation studied earlier. More specifically, we use the Néel initial state and compute the magnetization at site $i = 0$, the Hamming distance, and the return probability, and we use as localization indicators their asymptotic, steady-state values after a long time evolution for $t \sim 10^2 J_{\max}^{-1}$. In addition, we compute for each eigenstate the entanglement entropy associated with partitioning at the middle bond of the ion chain, and we use the entanglement entropy density averaged over all eigenstates as the fourth measure of localization.

In Figs. 4(a)-(c), we find that the three measures of collective state preservation all have a sigmoid-shaped dependence on disorder strength W. We can (arbitrarily) define for each measure an effective critical disorder W_c

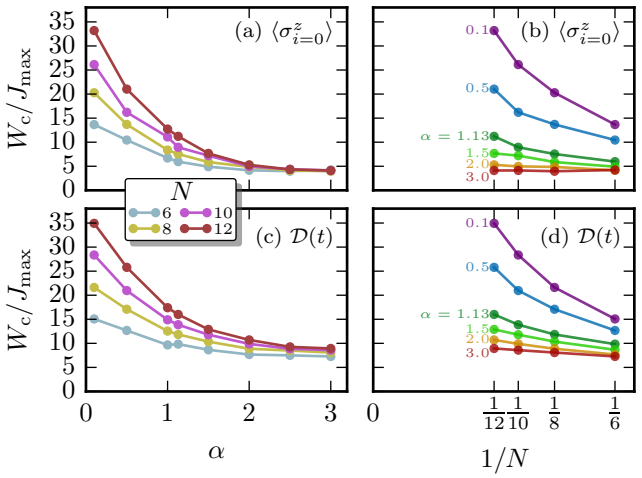

FIG. 5. Dependence of the effective critical disorder W_c on the long-range Ising exponent α, estimated by thresholding (a),(b) the steady-state magnetization at site $i = 0$, and (c),(d) the steady-state normalized Hamming distance. (a),(c) The α dependence for each system size N; (b),(d) the size N scaling grouped by α.

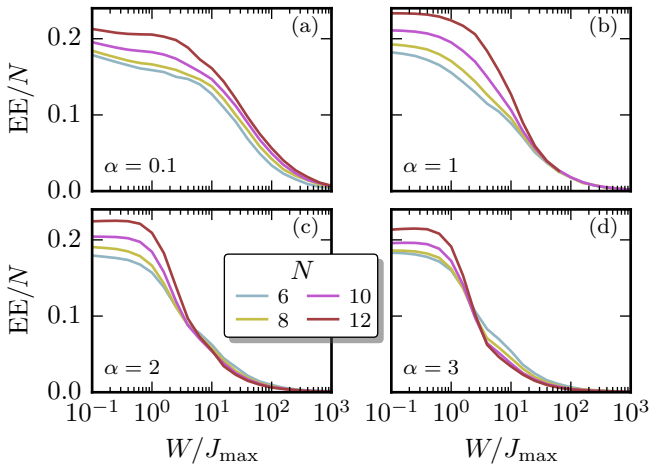

FIG. 6. Disorder dependence of entanglement entropy (EE) density for different values of the long-range Ising exponent α. Each data point shows the middle-cut entanglement entropy density.

at finite size, by thresholding at the halfway point of the sigmoid (indicated by the dotted line). For each of the three measures, we consistently find W_c in the vicinity of $10^1 J_{\max}$, although it exhibits an upward drift as system size N increases. This drift is most visible for the return probability, which may be partially attributed to overlap dilution from the exponential growth of the Hilbert space.

In Fig. 4(d), we find that for the trapped ions with long-range coupling exponent $\alpha = 1.13$, the middle-cut entanglement entropy on average exhibits an approximate volume law for $W \gtrsim 10^1 J_{\max}$, and at weaker disorder, the entanglement grows even faster as a function of system size N [24]. This behavior differs from the usual transition from volume law to area law as disorder increases in systems with short-range interactions. Nevertheless, the qualitative change in finite-size entanglement entropy scaling also occurs in the vicinity of $W_c \sim 10^1 J_{\max}$, in accordance with the change in other localization measures quantifying state preservation.

III. TUNING THE INTERACTION RANGE

So far we have focused on the $\alpha = 1.13$ point in the long-range regime of the disordered Ising model in order to stay close to the experimental results reported in Ref. [4]. In the following we move beyond the experimental setup and explore the effect of tuning α on the localization transition. Again, we characterize ergodicity breaking and localization using state preservation indicators and entanglement entropy.

Figure 5 shows the dependence of the effective critical disorder W_c on the exponent α and the system size N, determined by thresholding the state preservation indicators (as depicted in Fig. 4). Here we have skipped the return probability, given its particularly strong size dependence noted previously. At large α, the system has a clear localization transition, with the effective critical disorder W_c exhibiting only a weak size dependence. As α decreases, the localizing behavior is quickly and strongly suppressed. For $\alpha < 1$, the system resists localization until very strong disorder, and the critical W_c exhibits a clear size dependence, with no sign of convergence as N increases. Limited by the small system sizes, our results are not sufficient to confidently conclude whether the system still localizes in this parameter regime, but we do see a strong tendency towards delocalization, in contrast to the claim in Ref. [23]. This absence of localization for $\alpha < 1$ appears to obey Anderson's criterion [5] for single-particle localization with long-range hopping $t \sim 1/r^\alpha$ in one dimension, and it is also consistent with more refined analyses based on resonant pairs [25, 26], although much larger size numerics are needed to settle the regime with α slightly larger than one. It should also be noted that the effective strength of the long-range interaction relative to the on-site disorder is enhanced as system size increases, which may partially contribute to the growth of critical disorder as system size increases (Appendix A).

Figure 6 shows the disorder dependence of entanglement entropy density for various values of α. At large α, the Ising coupling is dominated by the nearest-neighbor part. Accordingly, for $\alpha = 3.0$ shown in Fig. 6(d), the eigenstates have on average an area-law entanglement entropy at strong disorder, and an approximate volume-law entanglement at weak disorder. This is the expected behavior for MBL systems with short-range interactions. As the Ising coupling range expands with decreasing α, the scaling of entanglement entropy grows steadily. For the intermediate value $\alpha \sim 1$, the entanglement in the strong disorder phase exhibits a volume-law decay to zero

as disorder increases. At very small α, the long-range Ising model completely loses its one-dimensional character and the entanglement entropy exhibits volume-law scaling for all disorder. Such dichotomy between small and large α is also visible in the dynamical growth of entanglement entropy (Appendix B).

IV. CONCLUSION

To conclude, we numerically examine the coherent dynamics of coupled qubits in the trapped-ion experiment reported in Ref. [4]. For the disordered Ising system with long-range couplings, we study in detail the experimental parameter setup and characterize the localizing behavior through collective state preservation and quantum entanglement. We observe semiquantitative agreement between the experimental data and our numerical results. We note that the strongest disorder probed in the experiment appears to be in the middle of the finite-size localization crossover. In addition, we have also explored the effect of tuning the long-range exponent α. For large α, the system exhibits a clear transition from a thermal phase at low disorder to a localized phase at strong disorder. For $\alpha < 1$, the effective critical disorder of the localization transition grows significantly as system size increases, indicating a possible absence of localization even at very strong disorder. This prediction should be tested in future experiments.

We thank C. Monroe, J. Smith, A. Lee, P. W. Hess, D.-L. Deng, and X. Li for useful discussions, and we thank P. Hauke and M. Heyl for alerting us to the interaction normalization issue. This work is supported by LPS-MPO-CMTC and NSF-JQI-PFC.

Appendix A: Alternative scaling analysis using the Kac prescription

In the main text, we discussed the scaling of various localization indicators with the system size N for the long-range Ising Hamiltonian,

$$H = J_{\max} \sum_{i<j} \frac{1}{|i-j|^\alpha} \sigma_i^x \sigma_j^x + \frac{1}{2} \sum_i (B + D_i) \sigma_i^z, \quad \text{(A1)}$$

and we noted that the scaling analysis may be affected by the dependence of the effective strength of the long-range coupling on the system size N. In the following, we address this point more carefully.

We consider a *different* model Hamiltonian for the trapped ions, using an alternative normalization scheme,

$$H_{\text{Kac}} = \frac{J}{\mathcal{N}_{N,\alpha}} \sum_{i<j} \frac{1}{|i-j|^\alpha} \sigma_i^x \sigma_j^x + \frac{1}{2} \sum_i (B + D_i) \sigma_i^z. \quad \text{(A2)}$$

Here, the normalization $\mathcal{N}_{N,\alpha}$ is given by the Kac prescription [27],

$$\mathcal{N}_{N,\alpha} = \frac{1}{N-1} \sum_{i<j} \frac{1}{|i-j|^\alpha}. \quad \text{(A3)}$$

This extra factor significantly enhances the effective strength of disorder relative to the Ising coupling as the system size increases. We pick $J = \mathcal{N}_{10,1.13} J_{\max}$ such that H_{Kac} coincides with H for the experimental system of $N = 10$ trapped ions.

We now examine the impact of the alternative normalization scheme on the scaling analysis. We compute for H_{Kac} the same set of localization measures as we did for H in the main text, and we use the same sigmoid-thresholding procedure to determine the localization crossover point. We plot in Fig. 7 the resulting dependence of the effective critical disorder W_c on the long-range exponent α and the system size N. We find that W_c grows only moderately as N increases, and it also does not exhibit a strong α dependence. The model Hamiltonian H_{Kac} thus appears to have a localization transition at finite disorder strength even for very small value of α. This is in sharp contrast to the unbounded growth of the critical W_c with increasing system size at small α in the absence of the Kac rescaling, as shown in Fig. 5 of the main text.

We emphasize that this qualitative change in ergodic or localizing behaviors stems from the different normalization schemes used in H and H_{Kac}. Conventional wisdom recommends the Kac prescription as it renormalizes the long-range coupling to have an extensive total energy. However, its relevance to the modeling of an ion-trap quantum simulator is debatable, since the exponent α is

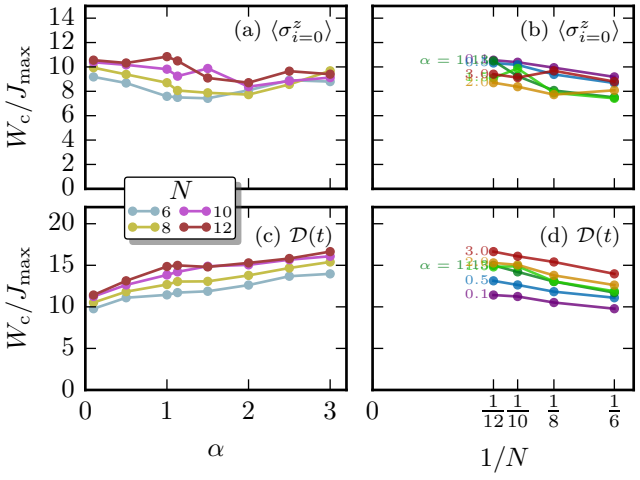

FIG. 7. Dependence of the effective critical disorder W_c on the long-range Ising exponent α for the alternative model Hamiltonian H_{Kac} [Eq. (A2)], estimated by thresholding (a),(b) the steady-state magnetization at site $i = 0$, and (c),(d) the steady-state normalized Hamming distance. (a,c) The α dependence for each system size N; (b,d) the size N scaling grouped by α.

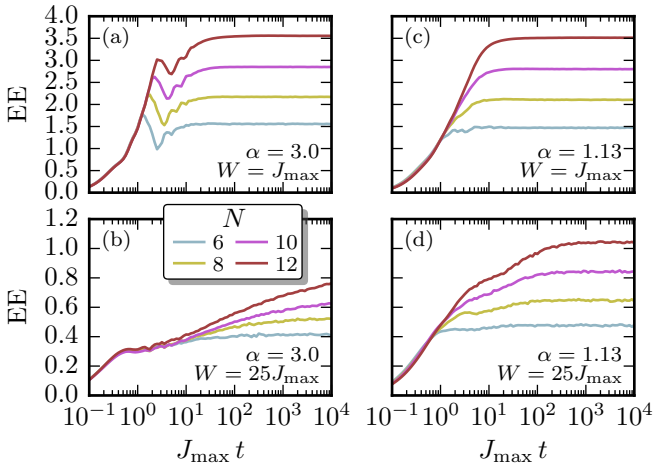

FIG. 8. Dynamical growth of entanglement entropy (EE) starting from the Néel state for (a),(b) short-range and (c),(d) long-range coupled systems at weak and strong disorder, respectively.

not an independent control variable that can be tuned separately from the system size N [4].

Appendix B: Dynamical entanglement growth

A hallmark of the *many-body* (as opposed to single-particle) localized phase of a local Hamiltonian is the logarithmic spreading of entanglement entropy [11, 12, 18]. In the following, we study such dynamical entanglement growth during the time evolution of the trapped ions. We use the Néel initial state $|\uparrow\downarrow \cdots \uparrow\downarrow\rangle_z$, and we compute entanglement entropy using the middle-cut partition detailed in the main text.

We start our analysis with the relatively simple, short-range coupled case at $\alpha = 3.0$, shown in Figs. 8(a) and (b). For weak disorder, we observe a linear growth of entanglement that quickly saturates to a value proportional to the system size N, consistent with a thermal phase. In contrast, for strong disorder such ballistic spreading of entanglement is superseded by a slow, logarithmic growth in the time window $1 \sim 10 J_{\max}^{-1}$, which is characteristic of many-body localization in short-range coupled systems. This further corroborates our claim that the disordered Ising Hamiltonian in the short-range interaction regime display a many-body localization transition.

The situation for the experimental system with long-range coupling ($\alpha = 1.13$) is less transparent. Comparing Figs. 8(c) and (d), we do not observe a qualitative distinction between strong and weak disorder. This apparent resistance against many-body localization for small α is consistent with our results obtained in the main text from analyzing the state preservation indicators and the eigenstate entanglement entropy. Quantitatively, we find that strong disorder still impedes the spreading of entanglement, but limited by the small system sizes, we are not able to identify the scaling behavior (linear, logarithmic, or power law [28]) of the entanglement growth as a function of time. It should be noted that such subtlety is a direct consequence of the long-range coupling between the trapped ions, and the experimental measurements of entanglement entropy will reflect exactly the same difficulties.

[1] R. Blatt and C. F. Roos, Nature Physics **8**, 277 (2012).
[2] C. Schneider, D. Porras, and T. Schaetz, Reports on Progress in Physics **75**, 024401 (2012).
[3] S. Lloyd, Science **273**, 1073 (1996).
[4] J. Smith, A. Lee, P. Richerme, B. Neyenhuis, P. W. Hess, P. Hauke, M. Heyl, D. A. Huse, and C. Monroe, ArXiv e-prints (2015), arXiv:1508.07026 [quant-ph].
[5] P. W. Anderson, Phys. Rev. **109**, 1492 (1958).
[6] D. M. Basko, I. L. Aleiner, and B. L. Altshuler, Annals of Physics **321**, 1126 (2006).
[7] I. V. Gornyi, A. D. Mirlin, and D. G. Polyakov, Phys. Rev. Lett. **95**, 206603 (2005).
[8] V. Oganesyan and D. A. Huse, Phys. Rev. B **75**, 155111 (2007).
[9] A. Pal and D. A. Huse, Phys. Rev. B **82**, 174411 (2010).
[10] J. Z. Imbrie, ArXiv e-prints (2014), arXiv:1403.7837 [math-ph].
[11] J. H. Bardarson, F. Pollmann, and J. E. Moore, Phys. Rev. Lett. **109**, 017202 (2012).
[12] M. Serbyn, Z. Papić, and D. A. Abanin, Phys. Rev. Lett. **110**, 260601 (2013).
[13] M. Serbyn, Z. Papić, and D. A. Abanin, Phys. Rev. Lett. **111**, 127201 (2013).
[14] R. Vosk and E. Altman, Phys. Rev. Lett. **110**, 067204 (2013).
[15] B. Bauer and C. Nayak, Journal of Statistical Mechanics: Theory and Experiment **2013**, P09005 (2013).
[16] D. A. Huse, R. Nandkishore, and V. Oganesyan, Phys. Rev. B **90**, 174202 (2014).
[17] E. Altman and R. Vosk, Annual Review of Condensed Matter Physics **6**, 383 (2015).
[18] R. Nandkishore and D. A. Huse, Annual Review of Condensed Matter Physics **6**, 15 (2015).
[19] D. J. Luitz, N. Laflorencie, and F. Alet, Phys. Rev. B **91**, 081103 (2015).
[20] M. Schreiber, S. S. Hodgman, P. Bordia, H. P. Lüschen, M. H. Fischer, R. Vosk, E. Altman, U. Schneider, and I. Bloch, Science **349**, 842 (2015).
[21] D. Porras and J. I. Cirac, Phys. Rev. Lett. **92**, 207901 (2004).
[22] It should be noted that the $J_{i,j}$ couplings as measured in the actual experiment in Ref. [4] deviate slightly from the power-law form. We find that our numerical results are not sensitive to such details.
[23] P. Hauke and M. Heyl, Phys. Rev. B **92**, 134204 (2015).
[24] We note that this apparently super-volume scaling of en-

tanglement entropy is visible only at finite size. This is consistent with the volume-law upper bound on the entanglement entropy from the Hilbert-space dimension.
[25] N. Y. Yao, C. R. Laumann, S. Gopalakrishnan, M. Knap, M. Müller, E. A. Demler, and M. D. Lukin, Phys. Rev. Lett. **113**, 243002 (2014).
[26] A. L. Burin, Phys. Rev. B **92**, 104428 (2015).
[27] M. Kac, G. E. Uhlenbeck, and P. C. Hemmer, Journal of Mathematical Physics **4**, 216 (1963).
[28] M. Pino, Phys. Rev. B **90**, 174204 (2014).